



Article Type : Research Article
Received : December 10, 2024
Revised : January 30, 2025
Accepted : February 13, 2025
DOI : [10.17798/bitlisfen.1599032](https://doi.org/10.17798/bitlisfen.1599032)

Year : 2025
Volume : 14
Issue : 1
Pages : 481-493



STUDY OF W+JET CROSS-SECTIONS AT NEXT-TO-LEADING ORDER AT FUTURE CIRCULAR COLLIDER AT $\sqrt{s}=100$ TEV

Gökhan HALİMOĞLU ^{1*} , Sehban KARTAL ¹ 

¹ *Istanbul University, Department of Physics, İstanbul, Türkiye*

* *Corresponding Author: g.halimoglu@iku.edu.tr*

ABSTRACT

This study provides a detailed investigation of $W + jets$ production in proton-proton collisions at $\sqrt{s} = 100$ TeV, focusing on the comparison of leading order and next-to-leading order cross-sections. By employing the UNLOPS algorithm, a unified framework was established to improve the accuracy and stability of theoretical predictions, particularly in the context of higher jet multiplicities. The k -factor, a critical metric for quantifying the impact of higher-order corrections, highlighted the substantial contributions of next-to-leading order processes compared to leading order, with a calculated value of 2.501. This value underscores the necessity of incorporating next-to-leading order corrections to achieve precise and reliable predictions in collider physics. The findings indicate that W^+ cross-sections are consistently higher than W^- cross-sections. Additionally, the differential cross-sections decrease as jet multiplicity increases, aligning with theoretical expectations.

This work emphasizes the importance of incorporating next-to-leading order corrections for future collider experiments, particularly for facilities like the future circular collider. The results provide a strong foundation for benchmarking theoretical predictions against experimental data and for guiding the optimization of next-generation colliders. Furthermore, the study highlights the versatility and robustness of the UNLOPS algorithm in addressing the challenges of high-energy jet dynamics, offering valuable insights into $W + jets$ processes and their role in advancing our understanding of Quantum Chromodynamics.

Keywords: FCC, WBoson, NLO, LO, Jets.

1 INTRODUCTION

The production of $W + jets$ has been a central focus in high-energy physics due to its importance in studying both the Standard Model (SM) and Beyond Standard Model (BSM) phenomena [1],[2]. Investigating the cross-sections of processes at leading order (LO) and next-to-leading order (NLO) provides essential insights, as NLO calculations significantly enhance the precision of theoretical predictions in high-energy physics [3][4]. Although many studies have been carried out at the Large Hadron Collider (LHC), exploring these processes for the future circular collider (FCC) remains highly significant [5].

To effectively explore $W + jets$ production at these energy scales, future collider facilities must be equipped with precise theoretical models. FCC is a next-generation collider project designed to push the frontiers of high-energy physics, with its first phase expected to be operational by 2035. The FCC is planned in multiple stages, including $FCC - ee$, an electron-positron collider for precision electroweak studies, followed by $FCC - hh$, a proton-proton collider aimed at exploring the highest energy regimes, and $FCC - eh$, an electron-proton collider for deep inelastic scattering investigations [5],[6].

Among these stages, $FCC - hh$ is particularly relevant to this study, as it is designed to operate at a center-of-mass energy of $\sqrt{s} = 100 TeV$, providing an unprecedented environment for studying high-energy jet processes. In such high-energy environments, accurate theoretical frameworks are required to interpret experimental data reliably. Precise k -factor calculations, along with differential and total cross-section predictions, are essential for optimizing theoretical models in such colliders.

The ability to accurately model jet multiplicities and kinematic distributions at these energy scales ensures reliable comparisons between experimental data and theoretical expectations, ultimately contributing to new physics searches [7].

To achieve this level of accuracy, perturbative QCD calculations must be systematically improved through higher-order corrections. Theoretical calculations in particle physics are systematically expanded in perturbative orders. Leading order (LO) represents the first-order approximation, capturing the dominant contributions in a given process. Next-to-leading order (NLO), on the other hand, incorporates second-order corrections, including virtual loop effects and additional real emissions, improving the precision of theoretical predictions. These refinements reduce scale uncertainties and enhance agreement with experimental

measurements, making them crucial for reliable cross-section evaluations. In high-energy collisions, such as those at $FCC - hh$, precise theoretical modeling is essential, and the k-factor serves as a key indicator of the impact of NLO corrections, ensuring more accurate comparisons between theory and experimental data. The k-factor, which is mathematically defined as:

$$k = \sigma_{NLO} / \sigma_{LO} \quad (1)$$

serves as an indicator of the relative contribution of NLO corrections compared to LO predictions. When the k-factor is close to unity, it suggests that LO calculations are sufficient for describing the process. However, k-factors point to the necessity of NLO corrections for achieving greater accuracy in theoretical predictions [8],[9].

Beyond evaluating theoretical precision, the k-factor is also used to assess the agreement between calculations and experimental measurements [9],[10]. If significant higher-order corrections are required to align with experimental data, this highlights the importance of refining the theoretical framework.

This study employs the UNLOPS algorithm alongside MadGraph, a versatile simulation tool that calculates tree-level matrix elements, cross-sections, and generates event samples [11],[12]. The UNLOPS algorithm, specifically designed for jet processes, integrates perturbative corrections across multiple jet multiplicities, offering a unified theoretical framework. This method is particularly advantageous for incorporating NLO and next-to-next-to-leading order ($NNLO$) corrections, especially in cases where the number of final-state jets varies. By combining contributions from LO and NLO levels for different jet multiplicities, the UNLOPS algorithm provides a more accurate and stable prediction framework. This approach is critical for minimizing non-perturbative effects during hadronization and ensuring better alignment of theoretical predictions with experimental outcomes.

Compared to other merging schemes, UNLOPS offers significant advantages in smoothly integrating fixed-order and parton-shower contributions. UNLOPS was selected over alternative merging algorithms, including MEPS@NLO and Powheg, due to its ability to facilitate a smoother transition across varying jet multiplicities while preserving NLO precision. Unlike MEPS@NLO, which predominantly employs exclusive phase-space slicing, UNLOPS adopts a more comprehensive approach to incorporating additional jet emissions. In contrast to Powheg, UNLOPS enables a more seamless integration of fixed-order matrix elements with parton showers, resulting in enhanced stability in differential cross-section computations [13].

By leveraging these theoretical advancements, this research provides key theoretical benchmarks for future collider experiments. Through the use of these advanced methods, including parton shower matching and merging techniques within the UNLOPS framework, this study contributes to enhancing the precision of $W + jets$ cross-section predictions, offering valuable insights for future collider experiments, particularly at FCC energies.

2 CALCULATIONS

The calculations were performed using the MadGraph software package and Pythia8 [10][14],[15] for parton shower simulations, incorporating both LO and NLO contributions

The parameters employed for the formation of all processes have been compared in the tables below.

Table1. The parameters for calculating cross-sections at LO and NLO levels have been delineated.

Parameter	LO Parton Level Samples	NLO Parton Level Samples
Energy	$\sqrt{s} = 100 \text{ TeV}; QCD$	$\mu F = mW$
Scales	$\mu R = \mu F = \mu ES = mW$	$\mu F = mW$
PDF	NNPDF23_lo_as_0130_qed	NNPDF23_nlo_as_0118_qed
Calculations	+0/1/2j @ LO and +0/1/2/3/4j @ LO	+0/1j @ NLO and +0/1/2j @ NLO
Parton Cuts	$pt_j > 0 \text{ GeV}; \eta_{tj} < 5.0;$ $BWC = \pm 15\Gamma$	$pt_j > 10 \text{ GeV}; BWC = \pm 15\Gamma$
Parton Shower	ickkw=0; xqcut=0.0; ptlund > 10 GeV	Pythia8; ickkw=4
Jet Clustering	Anti-kT; $dR=0.4$	Anti-kT; $dR=0.4$

The parameters used in this study are carefully chosen to ensure the accuracy and reliability of the simulated parton-level events at both LO and NLO . The center-of-mass energy (\sqrt{s}) is set to 100 TeV , representing a future collider scenario with high-energy QCD processes. The renormalization (μR) and factorization (μF) scales are dynamically defined using the W -boson mass (mW), minimizing theoretical uncertainties and improving the convergence of perturbative QCD predictions. For the parton distribution functions (PDFs), the NNPDF23_lo_as_0130_qed set is used for LO calculations, while NNPDF23_nlo_as_0118_qed is employed for NLO , providing a reliable description of parton momentum distributions within the proton.

The computational framework comprises two distinct configurations, namely Calculation I and Calculation II. This distinction allows for a systematic examination of jet activity across different perturbative orders, offering a clearer insight into the impact of higher-order corrections on differential cross-sections. Calculation I involve up to 2 jets at LO and 1 jet at NLO, whereas Calculation II extends the jet range to 4 jets at LO and 2 jets at NLO. To implement this framework, the simulation incorporates calculations covering a range of jet multiplicities, where LO samples account for processes with up to three additional jets (+0/1/2/3j/4j), while NLO samples include up to two additional jets (+0/1/2j).

The *NLO* samples are matched to parton showers using the *FxFx* merging scheme [12], which ensures a smooth transition between fixed-order matrix element calculations and parton shower simulations, thus avoiding double counting and improving event generation fidelity [15].

Jet clustering is performed using the anti-kT algorithm [16] with a radius parameter of $dR = 0.4$, which is widely recognized for its efficiency and stability in collider physics. Cuts on jet transverse momentum P_T^{jet} and pseudorapidity $|\eta|$ are applied to define the phase space, with stricter cuts imposed on *NLO* samples to enhance numerical stability [15].

Specifically, *NLO* samples require $P_T^{jet} \geq 10 \text{ GeV}$, while *LO* samples use a looser threshold. The Born-level Weight Cut (*BWC*) is consistently set to 15 across all simulations [17].

The parton shower for *NLO* events is simulated using Pythia8, with the merging process controlled by the *ickkw* parameter, which facilitates the proper integration of matrix-element and parton-shower contributions. When set to 0, no merging is performed, which is the standard setting for LO events. In contrast, for NLO events, *ickkw* is assigned a value of 4, enabling *FxFx* merging to establish a consistent connection between parton-level and shower-level emissions while preventing double counting errors. This configuration improves the precision and reliability of cross-section predictions, particularly in multi-jet processes, by ensuring an accurate representation of both hard scatterings and softer emissions, thereby capturing the intricate nature of *QCD* dynamics [18].

The comprehensive selection and implementation of these parameters are fundamental to achieving precise and reliable results, aligning with the goals of this study to provide a robust simulation framework for future collider experiments.

The aforementioned parameters and methods form the backbone of the simulations conducted in this study, ensuring consistency and precision in the cross-section calculations. The computational complexity involved in the multi-jet processes, particularly at *NLO*, necessitated significant computational resources. (*The simulations were performed on a high-performance workstation equipped with 128 GB of RAM and a 64-core 4 GHz processor*)

The entire process, which included matrix element computations, parton shower simulations, and merging, required approximately four weeks to complete. These resources underscore the computational demand of such detailed simulations, further emphasizing the importance of optimizing each parameter and method for accuracy and efficiency.

3 RESULTS AND DISCUSSION

The calculated cross-section values at both *LO* and *NLO* are systematically presented in the subsequent tables (Table 1, Table 2, and Table 3). These tables provide a comprehensive overview of the simulation results, highlighting the differences between *LO* and *NLO* predictions and their implications for the studied processes.

Table 2. Leading order cross-sections.

Sub-Process	$\sigma(W^+ \rightarrow \ell^+ \nu)$ [pb]	$\sigma(W^- \rightarrow \ell^- \nu)$ [pb]	Total Cross-section [pb]
$W^\pm(\rightarrow \ell^\pm \nu)+0j$	56253	51092	107340 ∓ 70.7
$W^\pm(\rightarrow \ell^\pm \nu)+1j$	49253	45520	94773 ∓ 111
$W^\pm(\rightarrow \ell^\pm \nu)+2j$	37351	34594	71946 ∓ 68
$W^\pm(\rightarrow \ell^\pm \nu)+3j$	25810	23745	49556 ∓ 99
$W^\pm(\rightarrow \ell^\pm \nu)+4j$	16217	14748	30965 ∓ 78

The cross-sections, expressed in picobarns (*pb*), calculated at leading order for various sub-processes are presented in Table 2. These calculations are based on a total of 100,000 generated events, ensuring statistical reliability in the results. These include processes with increasing jet multiplicities (*+0j, +1j, +2j, +3j, and +4j*). For each sub-process, the individual cross-sections for W^+ and W^- production, along with their sum as the total cross-section, are provided.

As observed, the total cross-section decreases systematically with increasing jet multiplicity. For instance, the $W + 0j$ process exhibits the highest total cross-section of 107340 ± 70.7 *pb*, whereas the $W + 4j$ process drops to 30965 ± 78 *pb*. This trend aligns with

expectations, as higher jet multiplicities correspond to increasingly suppressed phase-space regions and more complex interactions, leading to reduced cross-section values.

Additionally, the cross-sections for W^+ production are consistently higher than those for W^- across all sub-processes listed in Table 2. This disparity reflects the underlying asymmetry in parton distribution functions (*PDFs*) within the proton, where u -quarks, which predominantly contribute to W^+ production, are more abundant than d -quarks.

The uncertainties reported for the total cross-sections are minimal, indicative of the accuracy of the calculations and the efficiency of the simulation framework.

These results provide a foundational understanding of the parton-level dynamics at LO , serving as a benchmark for comparisons with NLO calculations and experimental data.

Table3. Next-to-leading order cross-sections.

Sub-Process	$\sigma(W^+ \rightarrow \ell^+ \nu)$ [pb]	$\sigma(W^- \rightarrow \ell^- \nu)$ [pb]	Total Cross-section [pb]
$W^\pm(\rightarrow \ell^\pm \nu)+0j$	146465	121959	268420 ∓ 1100
$W^\pm(\rightarrow \ell^\pm \nu)+1j$	95059	82654	177710 ∓ 1510
$W^\pm(\rightarrow \ell^\pm \nu)+2j$	60352	49900	110250 ∓ 2780

Table 3 showcases the cross-section results for processes with jet multiplicities ranging from $+0j$ to $+2j$ at NLO . These calculations are based on 50,000 generated events, ensuring statistical reliability in the results. As expected, the total cross-section decreases with increasing jet multiplicity, reflecting the growing complexity and phase-space restrictions associated with higher-order emissions. The total cross-section for $W + 0j$ is calculated as 268420 ± 1100 pb, while the value drops to 110250 ± 2780 pb for $W + 2j$.

A consistent pattern of higher cross-section values for W^+ production compared to W^- production is observed, attributed to the asymmetry in parton distributions within the proton. The simulations are based on a uniform event count across all sub-processes, ensuring statistical comparability. The relatively low uncertainties associated with the total cross-sections indicate the stability and reliability of the NLO simulations.

Table4. UNLOPS cross-sections and k-factor.

Inclusive cross-section [pb]		$k = \sigma_{nlo}/\sigma_{lo}$
LO	107345 ± 10734	2.501
NLO	268471 ± 13424	

Table 4 presents the inclusive cross-section values calculated at both *LO* and *NLO* using the UNLOPS merging scheme. The *NLO* cross-section 268471 ± 13424 pb is significantly higher than the *LO* cross-section 107345 ± 10734 pb, highlighting the enhanced precision and inclusion of higher-order corrections at the *NLO* level.

The k-factor, defined in Equation (1) as the ratio of the *NLO* cross-section to the *LO* cross-section, is calculated as 2.501. This value reflects the substantial contribution of *NLO* corrections to the overall cross-section and the importance of higher-order calculations in accurately modeling particle interactions.

These results demonstrate the robustness of the UNLOPS merging scheme in providing consistent and accurate predictions for inclusive cross-sections, which are crucial for both theoretical studies and experimental validations.

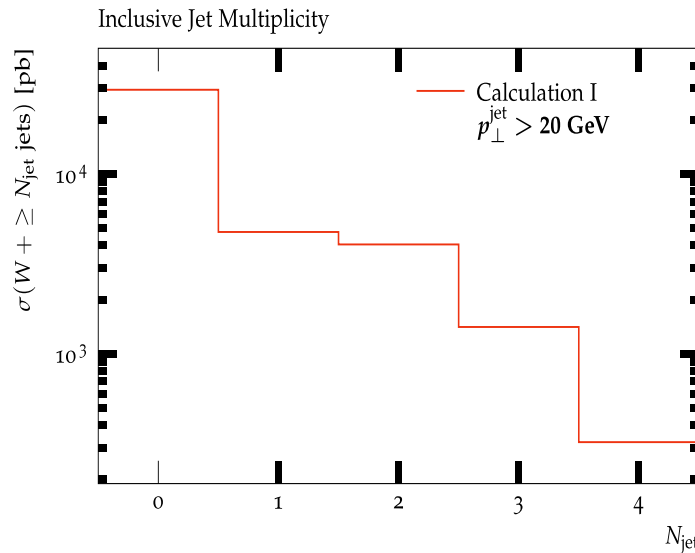


Figure1. Differential cross-sections are presented as a function of inclusive jet multiplicity ($P_T^{jet} > 20$ GeV) calculation I.

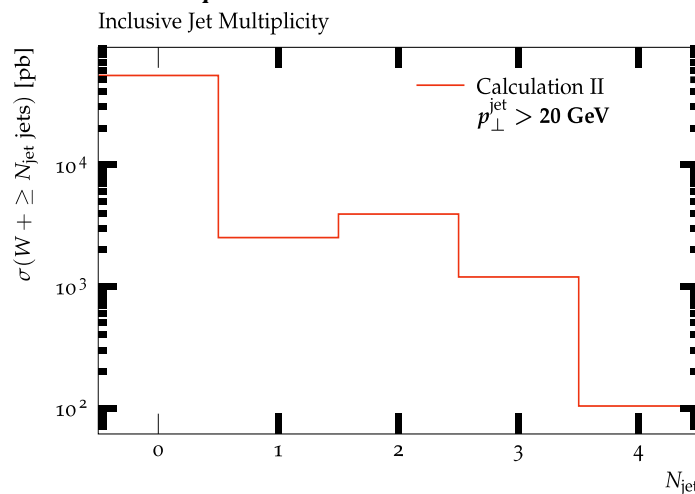


Figure2. Differential cross-sections are presented as a function of inclusive jet multiplicity ($P_T^{jet} > 20$ GeV) calculation II.

Figures 1 and 2 illustrate the differential cross-sections as a function of inclusive jet multiplicity N_{jet} for two distinct calculation methods, denoted as calculation I and calculation II. These plots provide a detailed comparison of the cross-section values for processes involving jets with $p_T^{jet} > 20 \text{ GeV}$. The stepwise decrease in cross-section with increasing N_{jet} is evident, reflecting the expected reduction in phase-space availability and the complexity of higher jet multiplicities.

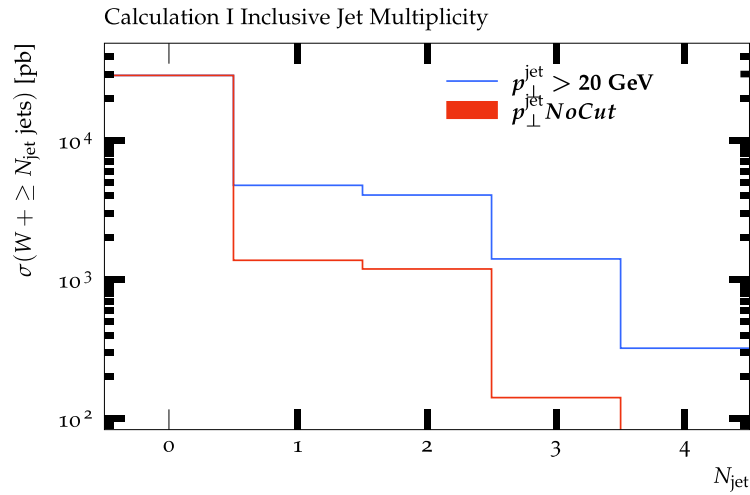


Figure3. Differential cross-sections as a function of inclusive jet multiplicity for Calculation I, comparing cases with and without a $p_{\perp}^{jet} > 20 \text{ GeV}$ cut.

Figure 3 focuses on calculation I and contrasts the cross-sections obtained with and without a transverse momentum cut $p_T^{jet} > 20 \text{ GeV}$. This comparison highlights the significant impact of applying such a cut, with noticeable differences in the inclusive cross-section values, particularly at higher jet multiplicities. This demonstrates the sensitivity of the results to jet kinematic cuts, which are crucial for aligning simulations with experimental conditions.

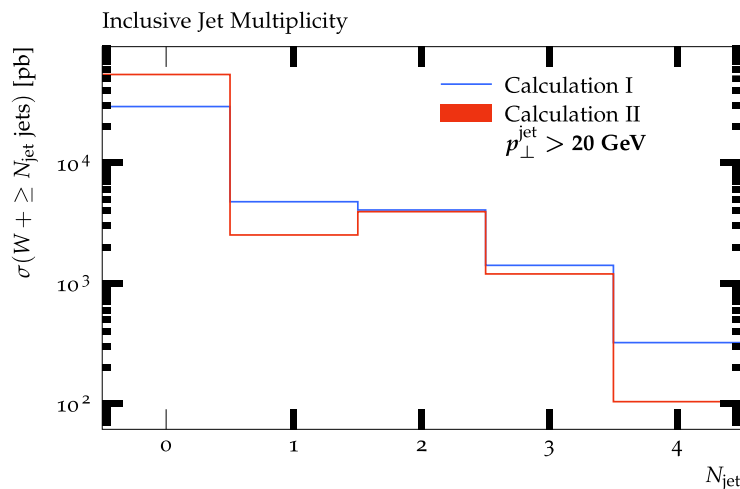


Figure4. The comparison of differential cross-sections is presented as a function of inclusive jet multiplicity for calculation I and calculation II.

Finally, Figure 4 provides a direct comparison of calculation I and calculation II, emphasizing the differences in the predicted cross-sections for identical kinematic configurations. The overlapping trends observed in lower multiplicities $N_{jet} = 0.1$ gradually diverge at higher N_{jet} , indicating the distinct approaches used in the two calculation methods. This comparison is instrumental in evaluating the consistency and reliability of the methodologies employed.

Collectively, these plots offer an in-depth view of the inclusive jet multiplicity distributions and their dependence on calculation strategies and jet kinematic cuts. These insights are essential for benchmarking theoretical predictions against experimental data and refining the computational frameworks for high-energy collider physics.

The presented results, combining the detailed cross-section values from Tables 1 to 4 and the visual insights from Figures 1 to 4, provide a comprehensive understanding of the studied processes. The tabulated data systematically highlight the impact of increasing jet multiplicities, where a clear reduction in total cross-sections is observed due to the constraints imposed by phase-space availability and higher-order jet emissions. This trend is consistently reflected in the plotted differential cross-sections, emphasizing the consistency of the simulations.

Additionally, the comparison of *LO* and *NLO* cross-sections across different jet configurations underscores the significance of higher-order corrections in achieving more accurate predictions. The k-factor values derived from Table 4 demonstrate the substantial enhancement provided by *NLO* calculations, further validating their necessity for precise modeling in high-energy collisions. The visual comparison in Figure 4 complements this finding by revealing how different calculation methods diverge in their predictions, especially at higher jet multiplicities.

The agreement between tabulated and plotted results not only reinforces the reliability of the simulation framework but also highlights the importance of careful parameter selection and methodological rigor. These findings serve as a strong foundation for benchmarking theoretical predictions against experimental data and for further studies aimed at refining computational models in particle physics.

4 CONCLUSION AND SUGGESTIONS

This study presents a comprehensive analysis of $W + jets$ processes, focusing on both inclusive and differential cross-sections as functions of jet multiplicities at LO , NLO , and UNLOPS merging schemes. The results offer significant insights into the interplay between jet multiplicities, higher-order corrections, and theoretical predictions, which are essential for accurate modeling of collider experiments at future facilities like $FCC - hh$, where the high-energy proton-proton collisions provide an ideal environment for studying QCD -driven jet dynamics.

Our findings confirm that, across all configurations, W^+ boson cross-sections are consistently higher than W^- boson cross-sections. This asymmetry arises from the dominance of $u - quark$ contributions within the proton, directly impacting W^+ production rates. Furthermore, the total cross-sections at NLO were systematically larger than at LO , with a calculated k-factor of 2.501, highlighting the necessity of incorporating higher-order corrections for reliable predictions. These results are in strong agreement with theoretical expectations, reinforcing the validity of our computational framework.

In addition, differential cross-sections exhibit a systematic decline with increasing jet multiplicities, reflecting the phase space suppression and computational challenges associated with higher-order emissions. The comparison between LO and NLO calculations reveals that NLO not only enhances precision but also offers a more robust theoretical foundation, particularly for final states involving 1–2 jets, where experimental uncertainties are critical. These findings emphasize the need for higher-order corrections to minimize theoretical uncertainties and align predictions with experimental observations.

A key aspect of this work is the implementation of the UNLOPS merging scheme, which enhances the reliability of theoretical predictions by ensuring a smooth transition between fixed-order matrix elements and parton showers. This merging strategy allows for a consistent treatment of high-energy and soft emissions, making it particularly valuable for inclusive jet multiplicity distributions at $FCC - hh$. Compared to other merging algorithms, UNLOPS provides improved stability in differential cross-section predictions, reinforcing its suitability for high-energy QCD studies.

To further refine these results, future studies should increase event statistics to 1 million, allowing for more precise evaluations of high-multiplicity jet events and reduced statistical uncertainties.

Beyond the scope of this study, exploring multi-boson production and heavy-flavor jet final states at $FCC - hh$ would offer deeper insights into $W + jets$ dynamics and new physics searches. These studies would not only aid in benchmarking theoretical frameworks but also support the development of experimental strategies for next-generation colliders.

Finally, to bridge the gap between theory and experiment, it is essential to incorporate experimental-level simulations, including detector effects and pile-up conditions. This would significantly enhance the applicability of our findings, ensuring that theoretical models are aligned with real collider data, ultimately contributing to the success of future $FCC - hh$ physics programs.

Conflict of Interest Statement

There is no conflict of interest between the authors.

Statement of Research and Publication Ethics

The study is complied with research and publication ethics.

Artificial Intelligence (AI) Contribution Statement

This manuscript was entirely written, edited, analyzed, and prepared without the assistance of any artificial intelligence (AI) tools. All content, including text, data analysis, and figures, was solely generated by the authors.

Contributions of the Authors

Gökhan Halimođlu: Led the formulation of the research question and conducted the literature review. Actively participated in data collection and analysis, performing statistical evaluations of the results. Additionally, Gökhan Halimođlu was responsible for drafting the initial manuscript and made substantial revisions to the entire text. Contributed significantly to the writing of the conclusions and the finalization of the manuscript.

Sehban Kartal: Provided overall guidance and conceptual direction for the study. Reviewed the manuscript drafted by Gökhan Halimođlu, offering academic mentorship and feedback. Contributed to the data analysis and provided guidance on the methodology section. Played a key role in the final revision of the manuscript, ensuring its quality and correcting writing errors.

REFERENCES

- [1] K. Öcalan, “Higher-order differential cross section calculation for the associated production of a W boson and jets in the electron decay channel at a center-of-mass energy of 13 TeV in proton-proton collisions,” *Turk J Phys*, vol. 43, pp. 156–166, 2019.
- [2] The ATLAS Collaboration, “Study of jets produced in association with a W boson in pp collisions at $\sqrt{s} = 7$ TeV with the ATLAS detector,” *Phys.Rev.D* 85 (2012) 092002.
- [3] J. M. Campbell, J. W. Huston, and W. J. Stirling, “Hard Interactions of Quarks and Gluons: a Primer for LHC Physics,” *Reports on Progress in Physics*, vol. 70, no. 1, pp. 89–193, Jan. 2007. [Online]. Available: <https://arxiv.org/abs/hep-ph/0611148>
- [4] [4K. Geiger and B. Müller, “QCD Evolution Equations for High Energy Partons in Nuclear Matter,” *Physical Review D*, vol. 50, no. 1, pp. 337–357, Jul. 1994. [Online]. Available: <https://doi.org/10.1103/PhysRevD.50.337>
- [5] M. Benedikt et al., “Future Circular Collider Study. Volume 3: The Hadron Collider (FCC-hh) Conceptual Design Report,” *Eur. Phys. J. ST*, vol. 228, no. 4, pp. 755–1107, 2019.
- [6] M. Benedikt and F. Zimmermann, Future Circular Collider Study. Volume 2: The Lepton Collider, CERN-ACC-2018-0057, CERN, Geneva, Switzerland, 2018. [Online]. Available: <https://cds.cern.ch/record/2651299>
- [7] M. Mangano et al., Future Circular Collider Study. Volume 1: Physics Opportunities, CERN-ACC-2018-0056, CERN, Geneva, Switzerland, 2018. [Online]. Available: <https://cds.cern.ch/record/2651305>
- [8] L. Lönnblad and S. Prestel, “Merging multi-leg NLO matrix elements with parton showers,” *Journal of High Energy Physics*, vol. 2013, no. 3, p. 166, 2013.
- [9] J. Alwall, R. Frederix, S. Frixione, V. Hirschi, F. Maltoni, O. Mattelaer, H.-S. Shao, T. Stelzer, P. Torrielli, and M. Zaro, “The automated computation of tree-level and next-to-leading order differential cross sections, and their matching to parton shower simulations,” *JHEP*, vol. 07, p. 079, 2014.
- [10] T. Sjöstrand, S. Ask, J. R. Christiansen, R. Corke, N. Desai, P. Ilten, S. Mrenna, S. Prestel, C. O. Rasmussen, and P. Z. Skands, “An introduction to PYTHIA 8.2,” *Computer Physics Communications*, vol. 191, pp. 159–177, 2015.
- [11] R. Frederix and T. Moskalets, “Five-flavour scheme predictions for $t\bar{t}b\bar{b}$ at next-to-leading order accuracy,” *European Physical Journal C*, vol. 84, no. 7, Article no. 763, Jul. 2024. Available: [arXiv:2403.14419](https://arxiv.org/abs/2403.14419)
- [12] S. Hoeche, F. Krauss, M. Schonherr, and F. Siegert, “QCD matrix elements + parton showers: The NLO case,” *Journal of High Energy Physics*, vol. 2013, no. 4, p. 27, 2013.
- [13] K. Hamilton and P. Nason, “Improving NLO-parton shower matched simulations with higher order matrix elements,” arXiv preprint arXiv:1004.1764, 2010. [Online]. Available: <https://arxiv.org/abs/1004.1764>
- [14] S. Catani et al., “Matching matrix elements and parton showers in hadronic collisions: The k_T-factorization approach,” *Journal of High Energy Physics*, vol. 2001, no. 5, p. 25, 2001.
- [15] M. Rubin, G. P. Salam, and S. Sapeta, “Giant QCD K-factors beyond NLO,” *Journal of High Energy Physics*, vol. 2010, no. 84, 2010.
- [16] M. Cacciari, G. P. Salam, and G. Soyez, “The anti-k_T jet clustering algorithm,” *Journal of High Energy Physics*, vol. 2008, no. 4, p. 63, 2008.
- [17] D. Kim, S. Lee, H. Jung, D. Kim, J. Kim, and J. Song, “A Panoramic Study of K-Factors for 111 Processes at the 14 TeV LHC,” arXiv preprint, arXiv:2402.16276, Feb. 2024. [Online]. Available: <https://doi.org/10.48550/arXiv.2402.16276>
- [18] J. Huston, “LO, NLO, LO* and jet algorithms,” *Proceedings of the Workshop on RadCor2009*, arXiv:1001.2581, Oct. 2010. [Online]. Available: <https://doi.org/10.48550/arXiv.1001.2581>.